Antagonism of Tumoral Prolactin Receptor Promotes Autophagy Related Cell Death

Yunfei Wen[1], Behrouz Zand[1], Bulent Ozpolat[2,6], Miroslaw J. Szczepanski[10], Chunhua Lu[1], Erkan Yuca[2], Amy R. Carroll[1], Neslihan Alpay[2], Chandra Bartholomeusz[3], Ibrahim Tekedereli[2], Yu Kang[1], Rajesha Rupaimoole[1], Chad V. Pecot[4], Heather J. Dalton[1], Anadulce Hernandez[12], Anna Lokshin[7], Susan K. Lutgendorf[8], Jinsong Liu[12], Walter N. Hittelman[2], Wen Y. Chen[9], Gabriel Lopez-Berestein[2,6], Marta Szajnik[11], Naoto T. Ueno[3], Robert L. Coleman[1,6], Anil K. Sood[1,4,5,6]*

Inventory of Supplemental Information

EXTENDED METHODS

Cell cultures

Human ovarian cancer cells HeyA8, A2780, and SKOV3 were cultured in RPMI 1640 cell culture medium supplemented with 15% fetal bovine serum (FBS) and 0.5% gentamicin (Halder et al., 2006; Lu et al., 2007). Human pancreatic cancer cells Pan-1 and HPAF2 were cultured in Dulbecco modified essential medium with 5% FBS. Mouse ovarian cancer cells IG10 were cultured in Dulbecco modified essential medium supplemented with 5% FBS and 1X Insulin-Transferrin-Sodium Selenite Supplement (Roche). Human prostate cancer cells LNcap were cultured in RPMI-1640 medium with 10% FBS. All cell lines were authenticated by the Cell Line Core Facility at The University of Texas MD Anderson Cancer Center and routinely tested to confirm the absence of *Mycoplasma*.

In vivo orthotopic models

Female athymic nude mice were used for the orthotopic tumor models. These animals were cared for according to guidelines set forth by the American Association for Accreditation of Laboratory Animal Care and the U.S. Public Health Service policy on Humane Care and Use of Laboratory Animals. All mouse studies were approved and supervised by The University of Texas MD Anderson Cancer Center Institutional Animal Care and Use Committee.

For *in vivo* orthotopic models, HeyA8 (2.5×10^5) or SKOV3ip1 (1×10^6) cells were inoculated into the peritoneal cavity; LNcap (4×10^6) cells were inoculated along with Matrigel. Seven days after inoculation, mice were randomized into one of four treatment

groups (n=10 mice/group): (1) vehicle control (mannitol, 100 μg/mouse, daily); (2) G129R (100 μg/mouse, daily); (3) paclitaxel (25 μg/mouse, weekly); or (4) G129R+paclitaxel at the same doses as for the single-agent treatments. The sample size (n=10) gave 80% power to detect a 50% reduction in tumor weight with 95% confidence. Mannitol, G129R, and paclitaxel were dissolved in phosphate-buffered saline solution (PBS) and administered intraperitoneally. Mice were monitored on a daily basis and weighed weekly. After 28 days of treatment, the mice were killed and the total body weight of each mouse, the numbers of tumor nodules, and their locations and weights were recorded. Tumor samples were fixed with 10% formalin and embedded in paraffin or with OCT compound in liquid nitrogen for sectioning and immunohistochemical assay.

For dose-finding experiments, SKOV3 tumor-bearing mice were treated with G129R at 100, 200, or 400 μg/mouse daily for 7 days.

For toxicity experiments, mice (n=5/group) were only treated with G129R at 100 μg/mouse, daily for 14 days.

Immunoblotting and antibodies

Immunoblotting analyses were performed as previously described (Halder et al., 2006). Briefly, cancer cells were plated at concentrations of 5×10^5 cells per 10-cm plate and treated with PRL, G129R, a combination (PRL+G129R), or control for 72 hours. Lysates were obtained by treating cells with a lysis buffer (Cell Signaling Technology, MA); aliquots containing 25 μg of total protein were subjected to separation by 10% Nu-PAGE gel electrophoresis (Life Technologies) and electrotransferred to nitrocellulose membranes. The membranes were blocked in Tris-buffered saline solution with 0.8%

Tween 20 containing 4% bovine serum albumin and were then probed with primary antibodies.

Antibodies against LC3 and beclin-1 were purchased from Cell Signaling Technology. Anti-PRLR-LF/ECD (1A2B1) antibody was purchased from Life Technologies. Anti-PRLR (clone BP774) for immunoblotting of prlr-ORF in PRLR-LF–null IG10 cells (Figure 5H) was purchased from Acris, Inc. (San Diego, CA). Anti-GHR for immunoblotting was purchased from Sigma Aldrich (St. Louis, MO), and anti-GHR for immunohistochemical staining was purchased from Abcam (Cambridge, MA). Antibodies against cleaved caspase-3, pY1007-1008–JAK2, JAK2, pY705-STAT3, STAT3, pY694-STAT5, STAT5, LC3-II, SQSTM1/p62, PEA-15, S104-phosphorylated PEA-15, T560-PKC-ζ, and PKC-ζ were purchased from Cell Signaling Technology. Antibodies against beta-actin and vinculin were obtained from Sigma Aldrich. Primary antibodies were diluted according to the manufacturer's instructions.

Tumor cell migration and invasion assays

Motility in the absence of a chemo-attractant (i.e., cell migration) was determined in membrane invasion culture system chambers that contained a polycarbonate filter with 10-μm pores coated with 0.1% gelatin, as previously described (Hendrix et al., 1987). HeyA8, SKOV3, and IG10 cells (7.5×10^4) that had been treated with PRL, G129R, or PRL+G129R or remained untreated (control) for 48 hours were seeded in each upper well and were incubated at 37°C for 6 hours in serum-free medium. The cells that migrated to the lower side of the membrane were processed by fixation with staining and were counted by examining five random fields per test condition. Image was taken at 100× magnification. Triplicate samples were measured for each condition and results

were averaged. Invasion assays were performed with 10-μm membrane transwell chambers as previously described (Landen et al., 2005). For the invasion assay, the time frame of incubation was extended to 16 hours.

AnnexinV and 7-AAD staining with flow cytometry

Apoptosis was evaluated by using the AnnexinV–phycoerythrin apoptosis detection kit according to the manufacturer's instructions (BD Biosciences). Each experiment was repeated three times.

Quantifying acidic vesicular organelles with acridine orange staining

The formation of acidic vesicular organelles (AVOs) was visualized by acridine orange (AO) staining (Paglin et al., 2001). In AO-stained cells, the cytoplasm or nucleolus fluoresces bright green and dim red, whereas acidic compartments fluoresce bright red. The volume of the cellular acidic compartment can be quantified on the basis of the intensity of the red fluorescence, which is proportional to the degree of acidity and/or the volume of the cellular acidic compartment (Akar et al., 2007). Green (510–530 nm) and red (>650 nm) fluorescence emissions from 1×10^4 cells illuminated with blue (488 nm) excitation light were measured by fluorescence-activated cell sorting (FACS) using a FACSCalibur from Becton Dickinson (Franklin Lakes, NJ) and CellQuest software (BD Biosciences).

Transmission electron microscopy

HeyA8 cells were grown in Matrigel-embedded conditions already described to create a 3-D spheroid structure and treated with PRL (0.5 μg/mL) or G129R (100 μg/mL) for 72 hours. Cells were fixed for 2 hours with 2.5% glutaraldehyde in 0.1 M cacodylate buffer (pH 7.4), fixed again in 1% OsO_4 in the same buffer, and then subjected to electron

microscopic analysis as described previously (Klionsky et al., 2008). Representative areas were chosen from ultra-thin sections; sections were viewed with a Hitachi 7600 electron microscope (Hitachi High Technologies America, Inc., Pleasanton, CA).

Tandem mRFP/mGFP-LC3 fluorescence microscopy

pGFP-RFP-LC3 (Addgene, Cambridge, MA) plasmids [9] were stably transfected into epithelial ovarian cancer cells (HeyA8, SKOV3). After 3-D culture on glass-bottom optical 35-mm^2 dishes (MatTek Corporation, Ashland, MA), expressed EGFP and RFP were visualized with a laser scanning multiphoton confocal microscope (TCS SP5 MP; Leica, Buffalo Grove, IL). To monitor autophagic flux in a high-throughout manner, RFP^+LC3–containing cells were analyzed by LSR Fortessa Flow Cytometry (BD Biosciences). Each experiment was repeated at least three times, and representative images from 15 high-power fields were identified.

Cell viability with MTT and live cells assay with SYTOX green

MTT assays were performed in 96-well plates using a Cell Proliferation Kit (Roche, Indianapolis, IN) following the manufacturer's instructions. Four to six wells were analyzed for each sample. The resulting colored solution was quantified using an ELx800 Absorbance Microplate Reader (BioTek, Winooski, VT) at 570 nm with a reference wavelength of 630 nm. SYTOX green staining (Invitrogen, Carlsbad, CA) was used to visualize dead cells according to the manufacturer's protocol. The population of SYTOX-positive dead cells was quantitated by FACS with 488 nm emission.

Immunohistochemical and histologic procedures

Tumor specimens from mice and human patients were first analyzed under a light microscope after hematoxylin and eosin (H&E) staining. Immunohistochemical analyses

of formalin-fixed, paraffin-embedded specimens were performed according to a published protocol (McCarty et al., 1985). The following primary antibodies were used for immunohistochemical analysis: polyclonal rabbit anti-human serine 104 (S104)-phosphorylated 15-kD astrocytic phosphoprotein (PEA-15), polyclonal rabbit anti-human cleaved caspase-3, monoclonal rabbit anti-human phosphorylated p62 (all purchased from Cell Signaling Technology); monoclonal mouse anti-human prolactin receptor (Thermo Fisher Scientific, Fremont, CA); rabbit polyclonal anti-human growth hormone receptor (GHR; Abcam Inc.); or appropriate isotype control IgG.

Immunohistochemical analyses of human epithelial ovarian tumors were conducted on 4-μm sections of formalin-fixed, paraffin-embedded specimens from human patients. After standard deparaffinization and rehydration, the LSAB+ kit (Dako, Gdynia, Poland) was used for staining according to the manufacturer's instructions. Antigen retrieval was performed using EDTA buffer (pH 9.0) in a 98°C water bath for 50 minutes followed by a 30-minute cooling to room temperature. Following antigen retrieval, endogenous peroxidases were blocked with 3% hydrogen peroxide in PBS (and methanol for p62) for 10 minutes at room temperature. To prevent nonspecific binding of the antibodies, tissue sections were incubated for 45 minutes with a serum-free protein blocker (Dako) at room temperature in a humid chamber before adding the primary antibodies. Sections were then incubated with primary antibodies overnight at 4°C. Secondary amplification was performed using the appropriate horseradish peroxidase–conjugated secondary antibody. Staining was visualized by application of 3,3′-diaminobenzidine (Dako). Slides were counterstained with hematoxylin (Sigma-Aldrich, Poznan, Poland) and mounted in mounting medium (Dako). Slides were evaluated on a light microscope

(100× or 200× magnification). Results were scored by two independent investigators (M.J.S. and M.S.). The sections were scored according to the percentage of tumor cells staining (POSITIVITY) (<25% = negative; 25‑75% = heterogenous; and >75% = positive). The level of staining (INTENSITY) was recorded as none = 0, weak = 1, moderate = 2, or strong = 3. The caspase-3 expression was scored according to the number of tumor cells staining (0 = 0-5; 1 = 5-20; or 2 = >20 positive cells) in five randomly chosen areas under 200× magnification.

Enzyme-linked immunosorbent assay of patient tumor homogenates and serum

Tumor tissue (100 mg per patient) was collected from surgical resection specimens of patients with epithelial ovarian cancer and frozen. The tissue was rinsed with 1× PBS and subjected to at least two cycles of freeze-thaw on dry ice to break the tissue and cell membranes. The homogenates were mechanically broken with a 10-mL Wheaton glass homogenization tube containing 1 mL of homogenization buffer (1× PBS). The homogenates were then subjected to centrifugation for 5 minutes at 14,000 rpm at 4°C. The supernatants were collected and aliquots analyzed by ELISA; the remaining supernatant was stored at -80°C for immunoblotting. Levels of PRL in supernatants were quantified with the use of a Quantikine Immunoassay kit (Prolactin ELISA, Cat# PR063F; CalBiotech, Springvalley, CA) according to the manufacturer's protocol. PRLR levels in the supernatants were quantified by Quantikine Immunoassay kit (Cat# DYC1167; R&D Systems, Minneapolis, MN). PEA-15 levels in the supernatants were quantified by a PEA15-ELISA kit (Cat# CSB-EL017764HU; Cusabio Biotech Co., Guandong, P.R.China). Levels of PRL, PRLR, PEA-15 (total and S104-phosphorylated),

and autophagic markers LC3-II and SQSTM1/p62 were examined by immunoblotting for validation.

Reverse-phase protein arrays

HeyA8 3-D cultured cells were treated with PRL, G129R, PRL+G129R, or control for 72 hours, and proteins were then extracted by using a lysis buffer containing the following: 1% Triton X-100, 50 nM HEPES (pH 7.4), 150 mM $MgCl_2$, 1 mM EGTA, 100 mM NaF, 10 mM sodium pyrophosphate, 1 mM Na_3VO_4, 10% glycerol, and freshly added protease and phosphatase inhibitors. Following instructions from the RPPA Process Core Facility at MD Anderson (http://bioinformatics.mdanderson.org/OOMPA), we arrayed these lysates on nitrocellulose-coated FAST slides (Whatman, Inc., Sanford, ME). Slides then were scanned and analyzed to quantitatively measure spot density to generate a fitted curve for each condition. The fitted curve was plotted with the log_2-concentration of proteins versus spot density. All data presented reflect fold-change compared to the baseline (i.e., to control-treated cells). Positive fold-change was calculated by dividing each linear value >1.0 by the average control linear value for each antibody tested, while negative fold-change (for linear values <1.0) was also calculated (using the following formula: [-1/linear fold-change]) and plotted in a heat map as a log 2.0 value.

cDNA microarray

Total RNA was extracted from HeyA8 cells cultured in 3-D Matrigel-embedded conditions with a mirVana RNA Isolation labeling kit (Ambion, Inc., Austin, TX). RNA purity was assessed by a Nanodrop spectrophotometric measurement (Thermo Scientific, Rockford, IL) of the OD260/280 ratio, with acceptable values falling between

1.9 and 2.1. Total RNA (300 ng) was used for labeling and hybridization on a Human HT-12 v4 Beadchip (Illumina, San Diego, CA) according to the manufacturer's protocols. After the bead chips were scanned with an Illumina BeadArray Reader, the microarray data were normalized using the quantile normalization method in the Linear Models for Microarray Data (LIMMA) software package in the R language environment. The expression level of each gene was transformed into a $\log_2$ base, and upregulated level was determined by comparison between the untreated control group and the G129R-treated group. Individual repeats of up to three groups were compared and upregulation -folds of $\log_2$ to 5-fold were included in the heatmap, created with Cluster v3.0 and Java TreeView v1.1.

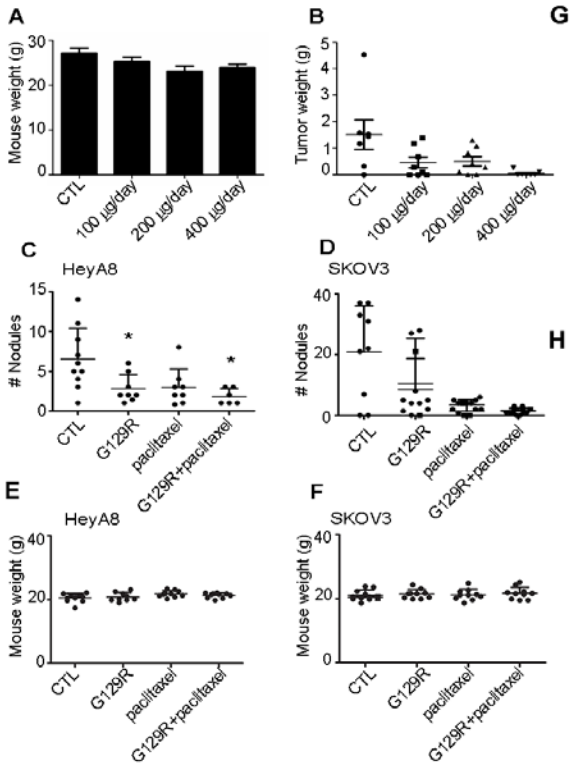

G

G129R (100μg/mouse/day)	Day 1	Day 3	Day 14
Complete CBC			
White Blood Cell (/μl)	$1.76*10^3$	$3.16*10^3$	$1.01*10^3$
Hemoglobin (g/dL)	13.9	12.9	14
Hematocrit (%)	44.8	42.8	45
Platelet Count (/μl)	$1.2*10^7$	$1.0*10^7$	$1.0*10^7$
Chemical Panel			
Alkaline Phosphatase(U/L)	187	91	84
ALT (SGPT)	47	37	34
AST (SGOT)	85	154	92
Ca 2+ (mg/dL)	9.5	9.6	9.3
Chloride (mEq/L)	115.2	113.3	113.6
K+ (mEq/L)	4.16	7.32	4.98
Na+(mEq/L)	149.1	174.5	149.4
Phosphorus (mg/dL)	5.1	7.2	7.2

H

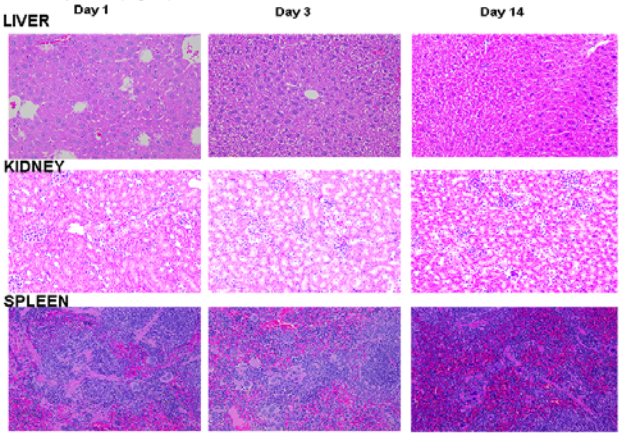

Supplemental Figure 1 (related to Figure 1). Dose effects and antitumor activity of G129R were assessed *in vivo* in orthotopic mouse models of human ovarian cancer.

(A,B) Effects of G129R at various doses on mouse weight and tumor weight. SKOV3 tumor-bearing mice were treated with a gradient dose (100, 200, or 400 μg/mouse daily) for 7 days. Mice were killed and the body weights (A) and tumor weights (B) were recorded.

(C,D) G129R, alone or in combination with paclitaxel, reduced the number of tumor nodules in tumor-bearing mice. Mice orthotopically injected with HeyA8 (C) or SKOV3 (D) ovarian cancer cells were randomized (n=10/group) to one of the following treatment regimens: control (CTL), G129R, paclitaxel, or G129R+paclitaxel. Numbers of tumor nodules for each treatment are shown. Error bars represent standard error of the mean;

*p<0.05 compared to the control group with one-way ANOVA. Mice treated with G129R or G129+paclitaxel had significantly fewer tumor nodules than mice in the control group in both HeyA8 (C) and SKOV3 (D) models.

(E,F) G129R and paclitaxel did not affect body weight of HeyA8 (E) or SKOV3 (F) tumor-bearing mice.

(G,H) Complete blood count (CBC) and chemistry panel (G) and H&E–stained images from liver, kidney, and spleen tissue samples (H) from mice treated with G129R 100 μg/mouse daily for 2 weeks. No significant toxic effects were observed from day 1 to day 14. Representative images were selected from three individual replicates. Magnification is 200×.

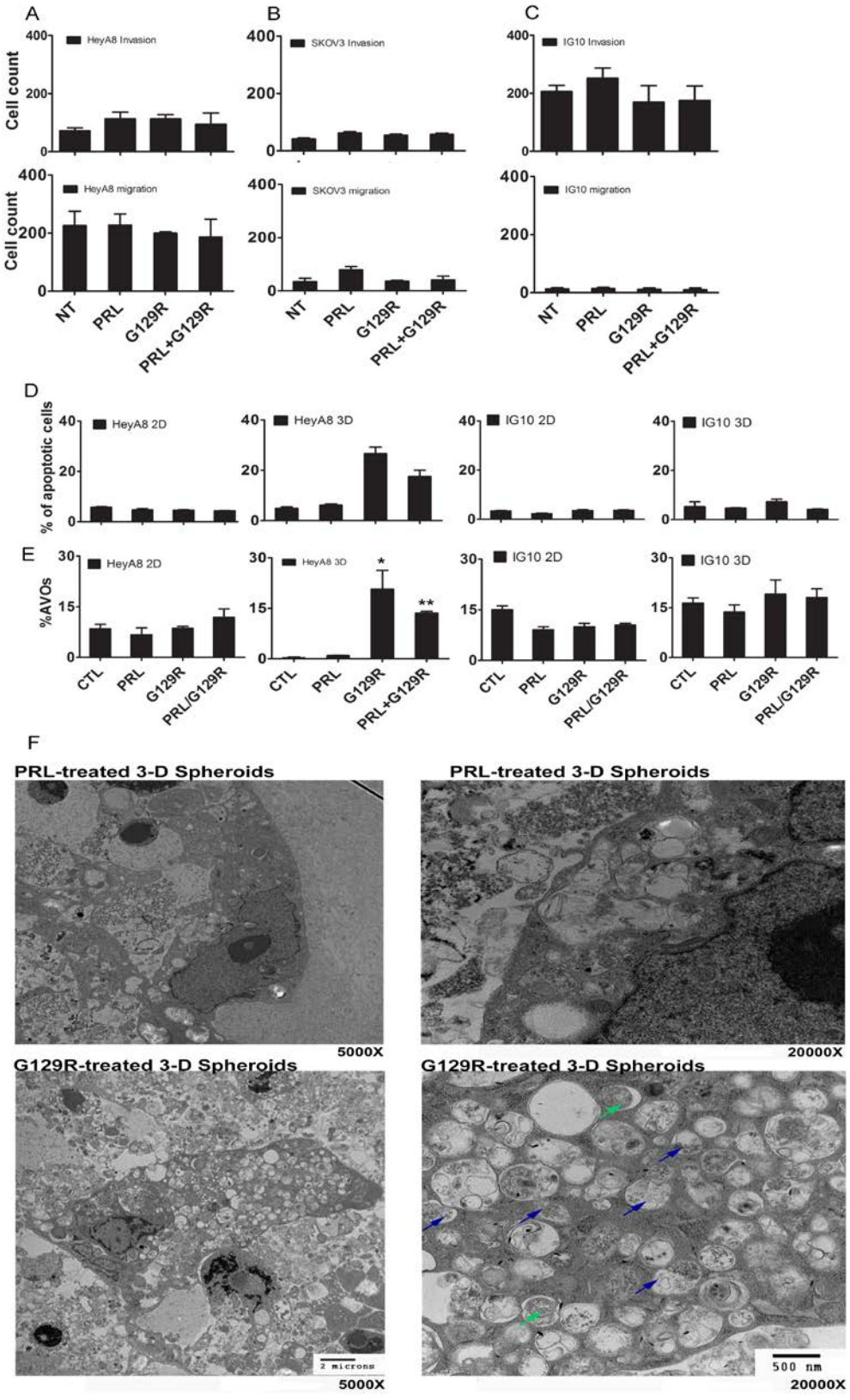
A
B
C
HeyA8 Invasion
SKOV3 Invasion
IG10 Invasion
HeyA8 migration
SKOV3 migration
IG10 migration
Cell count
NT
PRL
G129R
PRL+G129R
D
HeyA8 2D
HeyA8 3D
IG10 2D
IG10 3D
% of apoptotic cells
E
%AVOs
CTL
PRL/G129R
F
PRL-treated 3-D Spheroids
5000X
20000X
G129R-treated 3-D Spheroids
2 microns
500 nm

Supplemental Figure 2 (related to Figure 2 & Figure 3). G129R induced growth inhibition in cancer cells under 3-D culture conditions but not under 2-D conditions.

(A-C; related to Figure 2) G129R did not affect invasion and migration properties of cancer cells in 2-D arrays. HeyA8 (A), SKOV3 (B), and PRLR-LF–null IG10 (C) cells in 2-D monolayer cultures were treated with PRL, G129R, or PRL+G129R; controls were cells not treated (NT). (Upper panels) Mean numbers of invaded cells from five independent assays are shown. (Lower panel) Mean numbers of migrating cells from five independent assays are shown. Error bars represent the standard error of the mean. None of the 2-D cultured cancer cells showed significant changes in invasive or migration properties in response to G129R treatment.

(D; related to Figure 2) HeyA8 (left) and IG10 (right) cells were subjected to apoptosis assay using FACS with AnnexinV/7-AAD staining following culture in 2-D or 3-D conditions. Cells were treated with control (CTL), PRL, G129R, or PRL+G129R for 48 hours, and the percentage of apoptotic cells was defined as the AnnexinV-positive population.

(E; related to Figure 3) The percentage of AVOs HeyA8 (left) and IG10 (right) cells cultured under 2-D or 3-D conditions were measured by FACS with AO–staining. Cells were treated with CTL, PRL, G129R, or PRL+G129R for 72 hours.

Differences between groups in apoptosis (D) or autophagy (E) assays were compared by the unpaired two-tailed *t*-test; error bars represent standard error of the mean. In the autophagy assay (AVOs), **p*<0.0001 (CTL vs. G129R); ***p*<0.0005 (CTL vs. PRL+G129R).

(F; related to Figure 3) G129R induced enrichment of autophagic vacuoles in 3-D cancer spheroids. High-resolution images from transmission electron microscopy show autophagic vacuoles in isolated HeyA8 3-D cultured cancer spheroids treated with (upper panel) PRL 0.1 μg/mL or (lower panel) G129R 10 μg/mL for 72 hours. Autophagosomes (i.e., early autophagic vacuoles) are highlighted by the green arrows, and autolysosomes (i.e., late autophagic vacuoles) by the blue arrows (Klionsky et al., 2012)**.** Nuclear envelopes of selected cells are shown in left panels. Representative images were selected from 15 individual replicates. Magnifications are 5000× (left) and 20,000× (right).

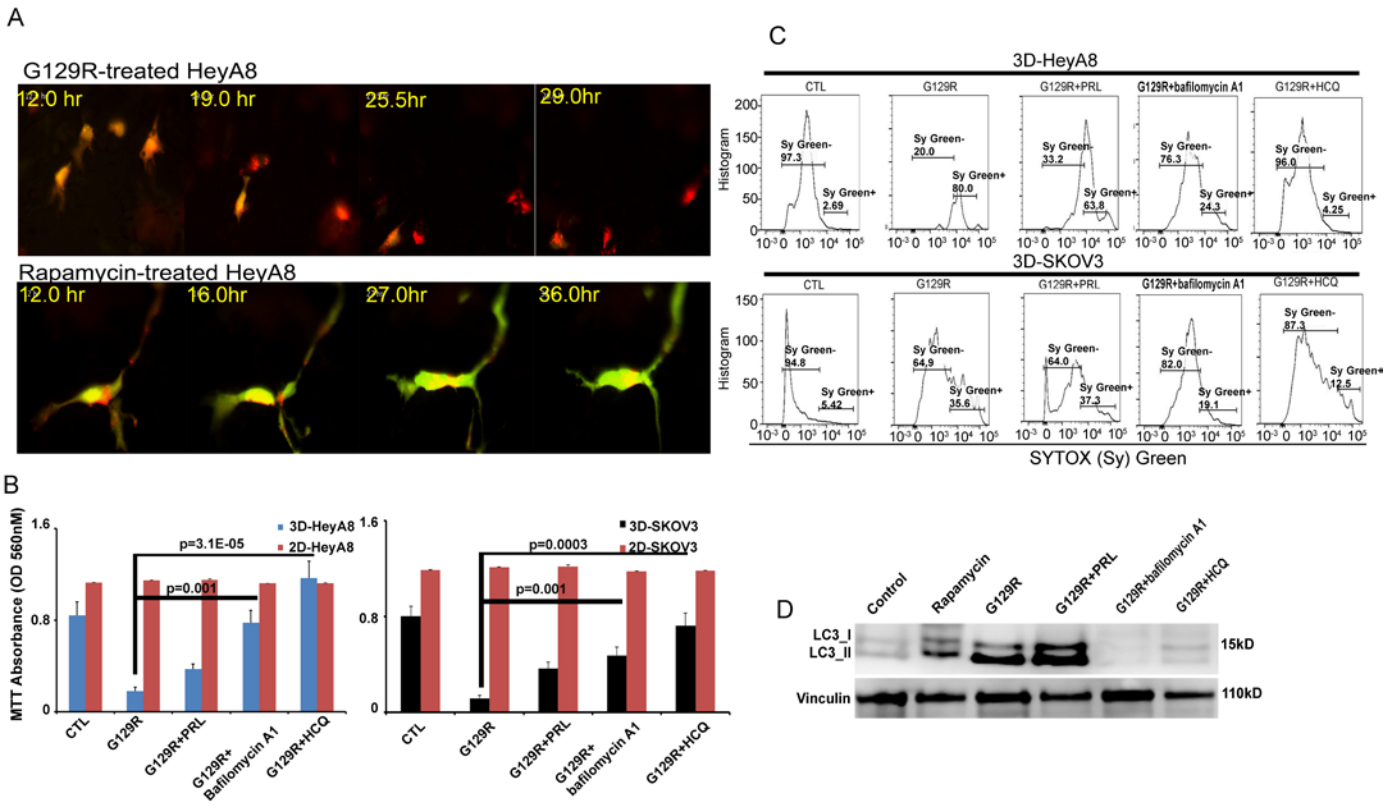

Supplemental Figure 3 (related to Figure 3). Cell death due to G129R-induced autophagy was reversed by autophagy inhibitors.

(A) 3-D HeyA8 spheroids expressing pGFP-RFP-LC3 were treated with G129R or rapamycin and the autophagic flux were monitored with real-time video microscopy. (Upper panel) Representative photomicrographs indicate the effect of G129R (10 μg/mL) at approximate elapsed times of 12, 19, 25, and 29 hours, showing the conversion of $GFP^{+and}RFP^{+}LC3$–containing cells to $RFP^{+only}LC3$. (Lower panel) Representative photomicrographs indicate the effect of rapamycin (50 nM) at approximate lapsed times of 12, 16, 27, and 36 hours, showing that the $GFP^{+and}RFP^{+}LC3$–containing cells remained stable (see Movies 5 & 6).

(B) Cell growth inhibition by G129R in 3-D cancer spheroids was reversed by autophagic inhibitors bafilomycin A1 and hydroxychloroquine (HCQ). HeyA8 and

SKOV3 cells were cultured in 2-D or 3-D conditions, and cell viabilities were assessed with the MTT assay. Cells were treated with control (CTL), G129R, PRL+G129R, G129R (72 hours)+bafilomycin A1 (0.16 nM for 24 hours), or G129R (72 hours)+hydroxychloroquine (HCQ, 1 nM for 24 hours), and the proportion of viable cells was determined by absorbance at OD570nm. Differences between groups were compared by unpaired two-tailed *t*-test. Values are mean+standard error (n=6). HeyA8: *p*=3.1E-05 (G129R vs. G129R+bafilomycin A1, 3-D); *p*=0.0001 (G129R vs. G129R+HCQ, 3-D). SKOV3: *p*=0.0003 (G129R vs. G129R+bafilomycin A1, 3-D); *p*=0.0001 (G129R vs. G129R+HCQ, 3-D).

(C) HeyA8 (upper panel) and SKOV3 (bottom panel) 3-D spheroids were treated with CTL, G129R, PRL+G129R, G129R (72 hours)+bafilomycin A1 (0.16 nM for 24 hours), or G129R (72 hours)+HCQ (1 nM for 24 hours), followed with SYTOX-green staining for detection of dead cells. Histograms showing results of FACS analysis are representative of three independent experiments. HeyA8 SYTOX-green positive: CTL, 2.69%; G129R, 80%; G129R+PRL, 63.8%; G129R+bafilomycin A1, 24.3%; G129R+HCQ, 4.25%. SKOV3 SYTOX-green positive: CTL, 5.42%; G129R, 35.6%; G129R+PRL, 37.3%; G129R+balifomycin A1, 19.1%; G129R+HCQ, 12.5%.

(D) Conversion of LC3-I to LC3-II in HeyA8 3-D spheroids was measured under the same conditions as in (B). Treatment with rapamycin (50 nM) for 24 hours was included as an autophagy positive control. Vinculin was included as loading control.

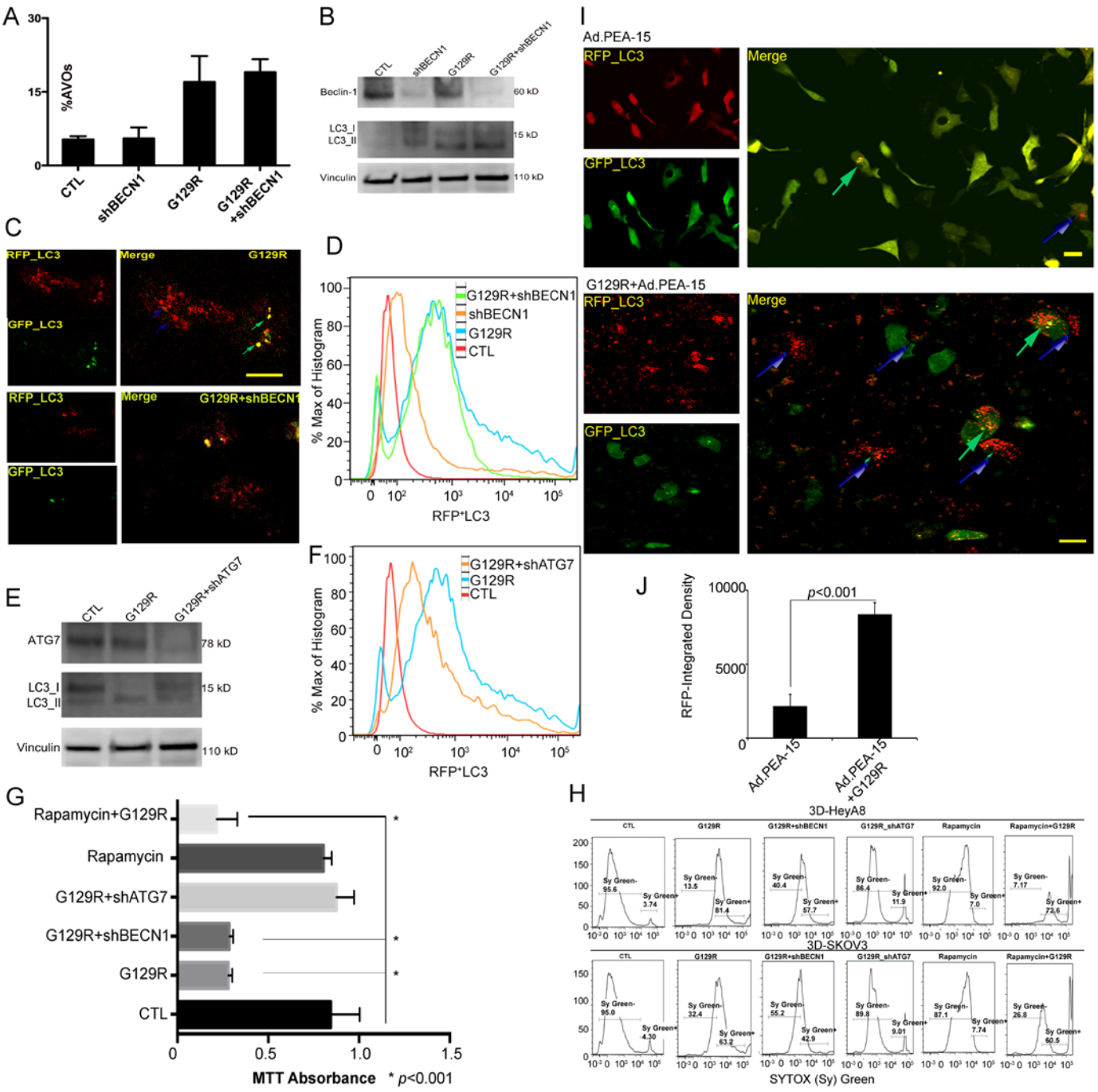

Supplemental Figure 4 (related to Figure 4). G129R-induced autophagy was independent of beclin-1 but mediated by PEA-15 and ATG7.

(A) 3-D HeyA8 spheroids treated with control (CTL) or transfected with shBECN1 were analyzed by FACS with AO to measure percentage of AVOs. There were no

significant differences between groups treated with G129R or G129R+shBECN1 for 72 hours. Differences between groups were compared by the unpaired two-tailed *t*-test; error bars represent standard error of the mean. $p>0.05$ (G129R vs G129R+shBECN1).

(B) Conversion of LC3-I to LC3-II was measured in 3-D HeyA8 spheroids treated with CTL, shBECN1, G129R, or G129R+shBECN1. shRNAs against BECN1 knocked down >95% of beclin-1 in HeyA8 3-D spheroids. The G129R-induced LC3-I/II conversion was not affected by shBECN1. Vinculin was included as loading control.

(C) Tandem mGFP/mRFP-LC3 fluorescence microscopy indicated that formation of autophagosomes (overlay of GFP-LC3 and RFP-LC3, as shown by green arrow) was induced by G129R in HeyA8 3-D parental or shBECN1-transfected cells. Knockdown of BECN1 did not alter the distribution of autolysosomes (RFP-LC3 only, as shown by blue arrow) induced by treatment with G129R. Representative images from 10 high-power fields are shown at magnification 400×. Scale bar = 20 μm.

(D) Histogram profile from FACS analysis with RFP^+ indicated there was no shift between G129R-treated and G129R+shBECN1–treated populations of 3-D HeyA8 spheroids.

(E) Conversion of LC3-I to LC3-II was measured in HeyA8 3-D spheroids treated with CTL, G129R, or G129R+shATG7. shRNAs against ATG7 knocked down >80% of ATG7 in HeyA8 3-D spheroids. In this case, G129R-induced LC3-I/II conversion was reversed by ATG7 knockdown to the level observed in CTL-treated cells. Vinculin was included as loading control.

(F) Histogram profile from FACS analysis with RFP^+ indicated a significant shift from G129R-treated to CTL-treated 3-D HeyA8 spheroids, whereas shATG7 knockdown reversed this shift.

(G) Cell viabilities of 3-D HeyA8 spheroids treated with control (CTL), G129R, G129R+shBECN1, G129R+shATG7, rapamycin (50nM), or rapamycin+G129R were assessed with the MTT assay. Differences between groups were compared by unpaired *t*-test. Values are mean+standard error (n=6). p=<0.001 (CTL vs. G129R, CTL vs. G129R+shBECN1, CTL vs. rapamycin+G129R).

(H) HeyA8 (upper panel) and SKOV3 (bottom panel) 3-D spheroids were treated with control (CTL), G129R, G129R+shBECN1, G129R+shATG7, rapamycin (50nM), or rapamycin+G129R, followed with SYTOX-green staining for detection of dead cells. Histograms showing results of FACS analysis are representative of three independent experiments. HeyA8 SYTOX-green positive: CTL, 3.74%; G129R, 81.4%; G129R+shBECN1, 57.7%; G129R+shATG7, 11.9%; rapamycin, 7.0%. rapamycin +G129R, 72.6%; SKOV3 SYTOX-green positive: CTL, 4.30%; G129R, 63.2%; G129R+shBECN1, 42.9%; G129R+shATG7, 9.01%; rapamycin, 7.74%. rapamycin +G129R, 60.5%.

(I) Tandem mGFP/mRFP-LC3 fluorescence microscopy indicated that autophagosomes containing both GFP^+LC3 and RFP^+LC3 were induced by Ad.PEA-15, while abundant autolysosomes containing RFP^+LC3 only were induced by G129R +Ad.PEA-15. Representative images from 10 high-power fields are shown at magnification 400×. (Upper) scale bar = 10 μm; (lower) scale bar = 20 μm.

(J) RFP^+-containing vesicles were quantitatively measured by fluorescence density in HeyA8 3-D spheroids treated with Ad.PEA-15 or G129R+Ad.PEA-15. Fifteen high-powe images were measured, and results were calculated as integrated density in comparison with background by unpaired two-tailed *t*-test: $p<0.001$ (G129R vs. G129R+ Ad.PEA-15).

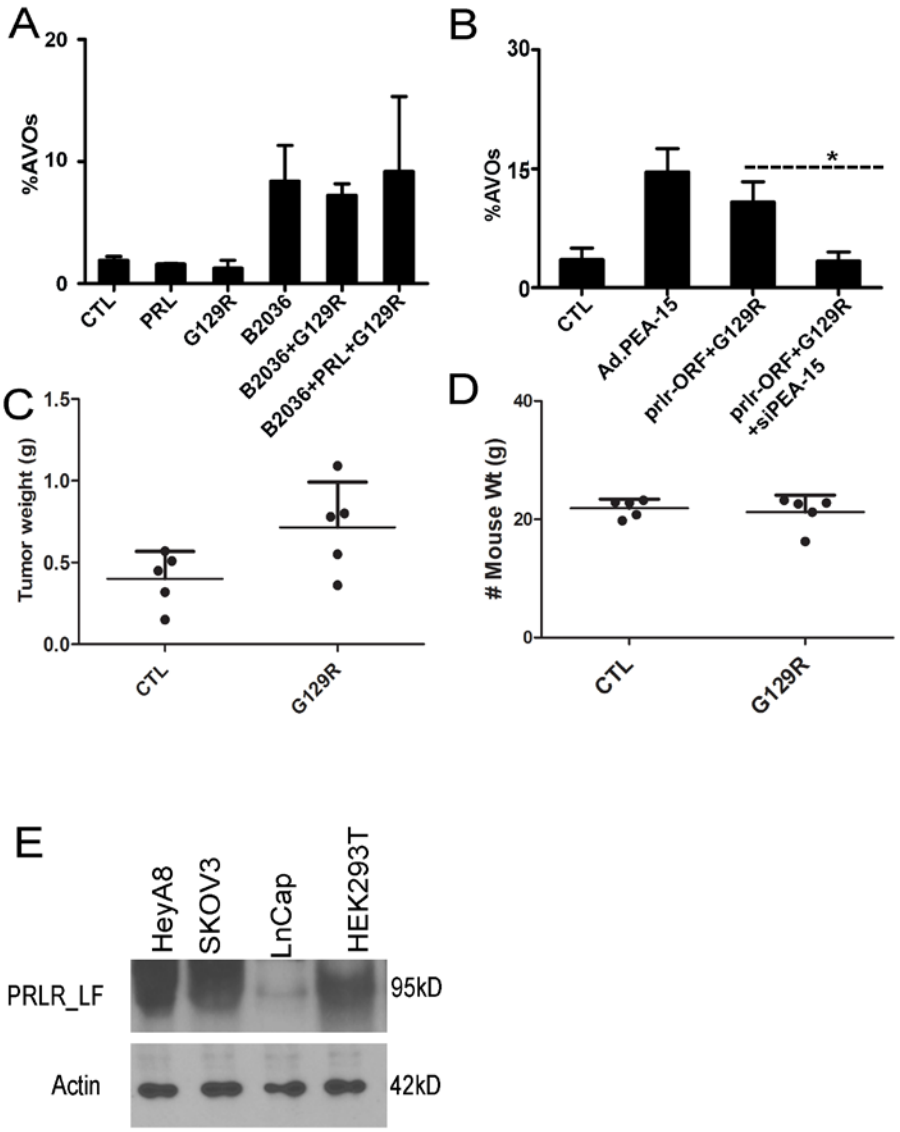

Supplemental Figure 5 (related to Figure 5). G129R specifically antagonized PRLR to inhibit tumor growth.

(A) GHR-specific inhibitor B2036, not G129R, induced autophagy in PRLR-deficient, GHR-positive LNcap cells**.** 3-D spheroids of LNcap cells (Xu et al., 2011) were treated with control (CTL), PRL, G129R, B2036, B2036+G129R, or PRL+B2036+G129R.

B2036 induced a prominent increase in the percentage of AVOs, while G129R had no significant effect.

(B) Overexpression of prlr-ORF restored the G129R-induced autophagy in LNcap 3-D spheroids, but knockdown of PEA-15 by siPEA-15 reversed this effect.

LNcap were treated with CTL, Ad.PEA-15, G129R+*prlr*-ORF, or G129R+*prlr*-ORF+siPEA-15. Overexpression of PEA-15 or prlr-ORF reconstituted the inducible autophagy (reflected by the percentage of AVOs). Knockdown of PEA-15 significantly decreased the autophagy induced by G129R+*prlr*-ORF. Differences between groups were compared by the unpaired two-tailed *t*-test, **p*<0.05.

(C,D) G129R did not inhibit tumor growth of PRLR-null LNcap cells *in vivo.* Mice orthotopically injected with LNcap cells were treated with mannitol as CTL or G129R (100 μg/mouse intraperitoneally daily). After 21 days of treatment, mice were killed and their tumor weight (C) and body weight (D) were recorded. There was no significant difference in tumor weight or mouse body weight between the two groups.

(E) The expression of PRLR-LF was verified in HeyA8, SKOV3, LNcap, and HEK293T cells.

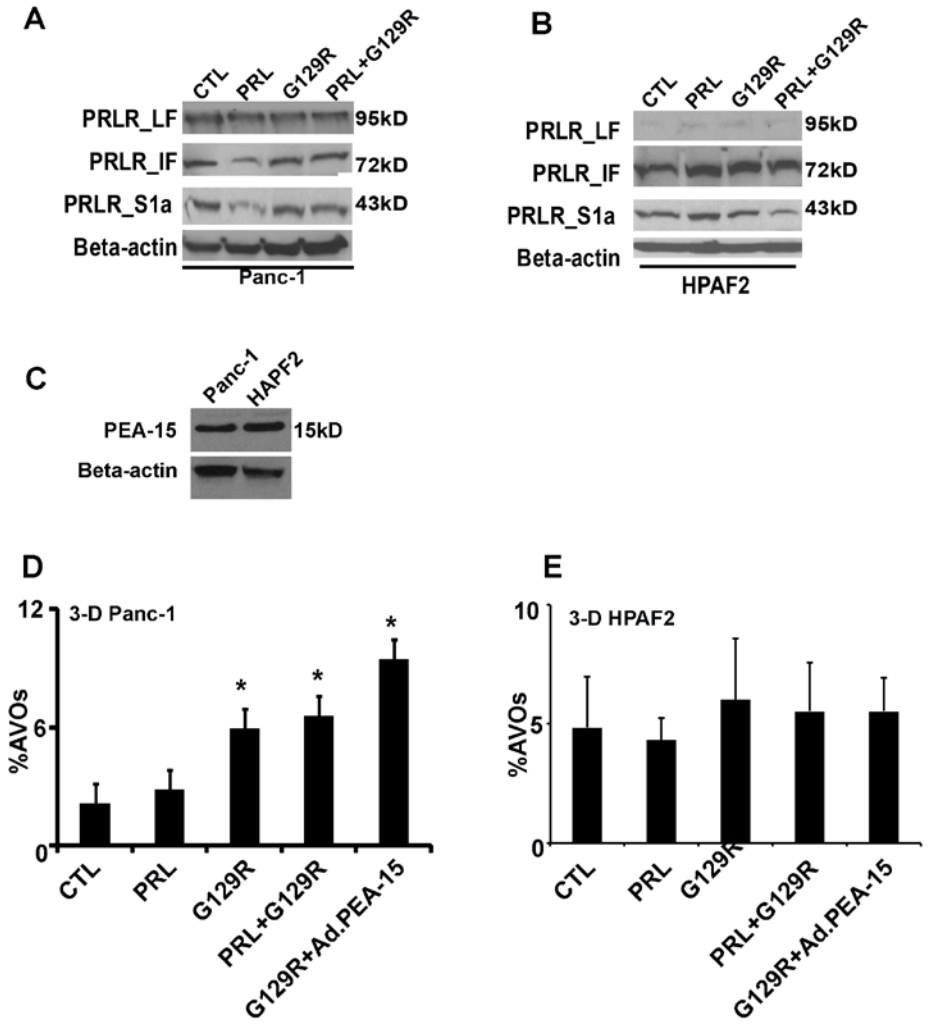

Supplemental Figure 6 (related to Figure 5). G129R induced autophagy in Panc-1 human pancreatic cancer cells but not in PRLR-LF–deficient HPAF2 cells.

(A,B) Expression of different isoforms of PRLR in human pancreatic carcinoma cells Panc-1 (A) and HPAF2 (B): PRLR long form (PRLR-LF, 95 kDa) was expressed in Panc-1 cells but not in HPAF2 cells.

(C) PEA-15 was expressed in both Panc-1 and HPAF2.

(D,E) Percentage of AVOs formed in Panc-1 (left) or HPAF2 (right) 3-D spheroids treated with PRL, G129R, PRL+G129R, or G129R+Ad.PEA-15 was assessed by FACS analysis with AO. In Panc-1 cells, the numbers of AVOs formed in response to G129R, PRL+G129R, or G129R+Ad.PEA-15 were significantly higher than those formed in response to CTL or PRL, while the differences in AVO formation in HPAF2 were not significant. Differences between groups were compared with the unpaired two-tailed *t*-test; error bars represent standard error of the mean; *$p<0.05$ (CTL vs. G129R, PRL+G129R, or G129R+Ad.PEA-15).

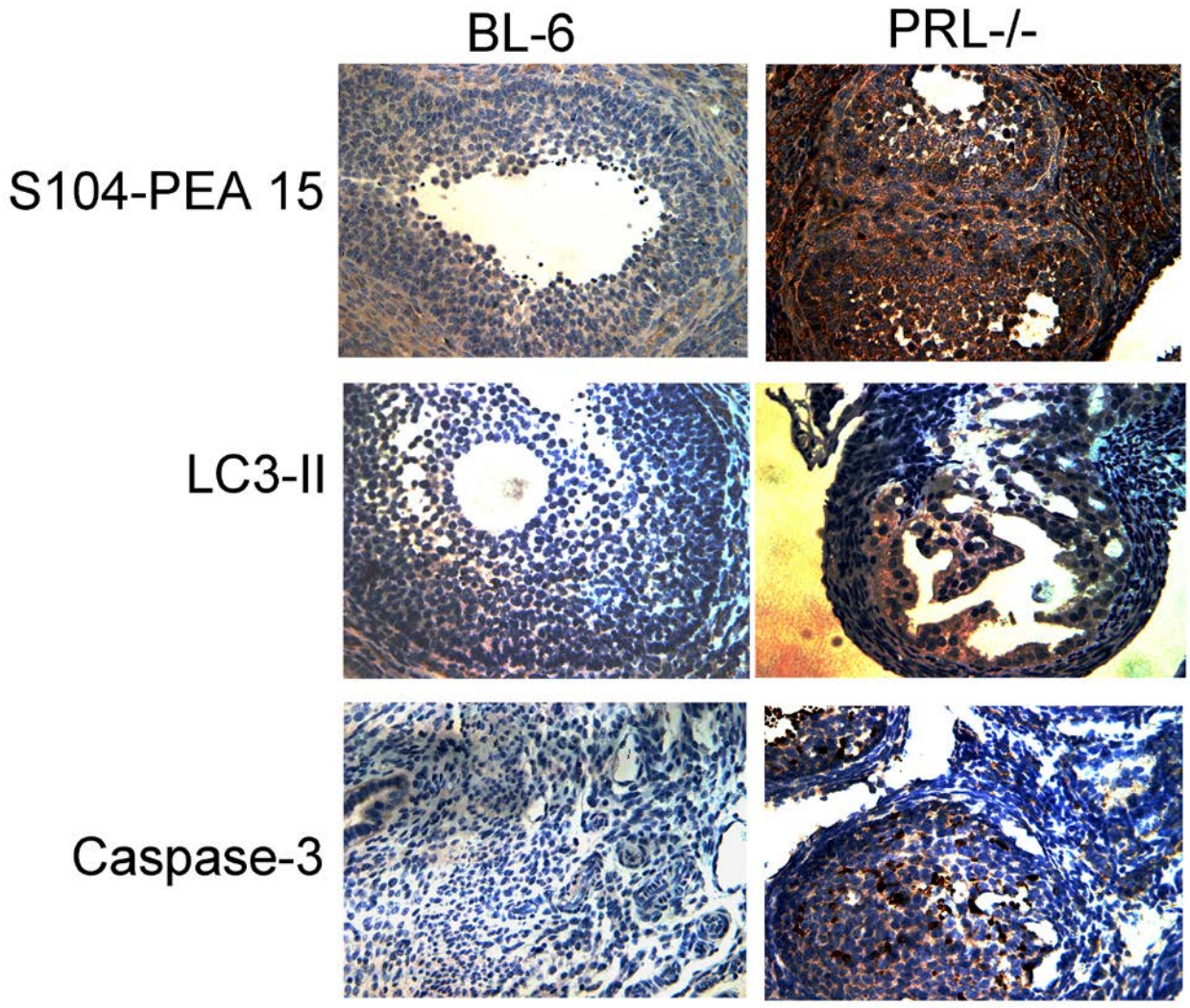

Supplemental Figure 7 (related to Figure 6). Expression of phosphorylated pS104-PEA-15, caspase-3, and LC3-II were higher in mice with PRLR deficiency.

Higher levels of phosphorylated PEA-15 (pS104-PEA-15), LC3-II and activated caspase-3 expressed in PRLR-deficient mice than what in BL6 wild-type. Ovarian tissues of PRL-deficient or BL6 wild-type female mice aged 4 weeks (n=3/group) were subjected to immunohistochemical staining of PEA-15 (S104-phosphorylated), LC3-I/II,

or cleaved caspase-3. PRL deficiency increased the levels of these three proteins, which are involved in autophagic cell death.

Supplementary Table 1 related to Figure 7.

Table S1. Clinical and pathological characteristics of epithelial ovarian cancer patients (n=32)

		Frequency
Menopausal Status	Pre-menopausal	15
	Post-menopausal	17
FIGO Stage	I	3
	II	4
	III	23
	IV	2
Tumor Grade	Low	1
	High	31
Cytoreduction	Optimal	12
	Sub-optimal	20
Number of Recurrences	0	6
	1	17
	>2	6
	No remission	3
Vital Status	Alive	20
	Dead	12

Movie S1. Related to **Figure 2D**. Live video microscopy of HeyA8 3-D ovarian cancer spheroids under untreated conditions (CTL). Image-capture interval was every 20 minutes over ~3000 minutes.

Movie S2. Related to **Figure 2D.** Live video microscopy of HeyA8 3-D ovarian cancer spheroids treatd with PRL 0.1 μg/mL (PRL). Image-capture interval was every 20 minutes over ~3000 minutes.

Movie S3. Related to **Figure 2D.** Live video microscopy of HeyA8 3-D ovarian cancer spheroids treated with G129R 10 μg/mL (G129R). Image-capture interval was every 20 minutes over ~3000 minutes.

Movie S4. Related to **Figure 2D.** Live video microscopy of HeyA8 3-D ovarian cancer spheroids treated with combination of PRL and G129R (PRL+G129R). Image-capture interval was every 20 minutes over ~3000 minutes.

Movie S5. Related to **Figure 3J & 3K.** Live video microscopy of HeyA8 ovarian cancer cells treated with G129R (10 μg/mL). Image-capture interval was every 30 minutes over 30 hours.

Movie S6. Related to **Figure 3J & 3K.** Live video microscopy of HeyA8 ovarian cancer cells treated with rapamycin (50 nM). Image-capture interval was every 30 minutes over 39 hours.

References

Akar, U., Ozpolat, B., Mehta, K., Fok, J., Kondo, Y., and Lopez-Berestein, G. (2007). Tissue transglutaminase inhibits autophagy in pancreatic cancer cells. Mol Cancer Res 5, 241-249.

Halder, J., Kamat, A. A., Landen, C. N., Jr., Han, L. Y., Lutgendorf, S. K., Lin, Y. G., Merritt, W. M., Jennings, N. B., Chavez-Reyes, A., Coleman, R. L., et al. (2006). Focal adhesion kinase targeting using in vivo short interfering RNA delivery in neutral liposomes for ovarian carcinoma therapy. Clinical cancer research : an official journal of the American Association for Cancer Research 12, 4916-4924.

Hendrix, M. J., Seftor, E. A., Seftor, R. E., and Fidler, I. J. (1987). A simple quantitative assay for studying the invasive potential of high and low human metastatic variants. Cancer letters 38, 137-147.

Klionsky, D. J., Abdalla, F. C., Abeliovich, H., Abraham, R. T., Acevedo-Arozena, A., Adeli, K., Agholme, L., Agnello, M., Agostinis, P., Aguirre-Ghiso, J. A., et al. (2012). Guidelines for the use and interpretation of assays for monitoring autophagy. Autophagy 8, 445-544.

Klionsky, D. J., Abeliovich, H., Agostinis, P., Agrawal, D. K., Aliev, G., Askew, D. S., Baba, M., Baehrecke, E. H., Bahr, B. A., Ballabio, A., et al. (2008). Guidelines for the use and interpretation of assays for monitoring autophagy in higher eukaryotes. Autophagy 4, 151-175.

Landen, C. N., Kinch, M. S., and Sood, A. K. (2005). EphA2 as a target for ovarian cancer therapy. Expert Opin Ther Targets 9, 1179-1187.

Lu, C., Kamat, A. A., Lin, Y. G., Merritt, W. M., Landen, C. N., Kim, T. J., Spannuth, W., Arumugam, T., Han, L. Y., Jennings, N. B., et al. (2007). Dual targeting of endothelial cells and pericytes in antivascular therapy for ovarian carcinoma. Clinical cancer research : an official journal of the American Association for Cancer Research 13, 4209-4217.

McCarty, K. S., Jr., Miller, L. S., Cox, E. B., Konrath, J., and McCarty, K. S., Sr. (1985). Estrogen receptor analyses. Correlation of biochemical and immunohistochemical methods using monoclonal antireceptor antibodies. Archives of pathology & laboratory medicine 109, 716-721.

Paglin, S., Hollister, T., Delohery, T., Hackett, N., McMahill, M., Sphicas, E., Domingo, D., and Yahalom, J. (2001). A novel response of cancer cells to radiation involves autophagy and formation of acidic vesicles. Cancer research 61, 439-444.

Xu, J., Zhang, Y., Berry, P. A., Jiang, J., Lobie, P. E., Langenheim, J. F., Chen, W. Y., and Frank, S. J. (2011). Growth hormone signaling in human T47D breast cancer cells: potential role for a growth hormone receptor-prolactin receptor complex. Mol Endocrinol 25, 597-610.